Quantum Spin Excitations through the metal-to-insulator crossover in $YBa_2Cu_3O_{6+y}$

Shiliang Li,[1,*] Zahra Yamani,[2] Hye Jung Kang,[3,4] Kouji Segawa,[5]
Yoichi Ando,[6] Xin Yao,[7] H. A. Mook,[8] and Pengcheng Dai[1,8,†]

[1] *Department of Physics and Astronomy, The University of Tennessee, Knoxville, Tennessee 37996-1200, USA*
[2] *Canadian Neutron Beam Centre, National Research Council, Chalk River Laboratories, Chalk River, ON K0J 1J0, Canada*
[3] *NIST Center for Neutron Research, National Institute of Standards and Technology, Gaithersburg, Maryland 20899-8562, USA*
[4] *Department of Materials Science and Engineering, University of Maryland, College Park, Maryland 20742-6393, USA*
[5] *Central Research Institute of Electric Power Industry, Komae, Tokyo 201-8511, Japan*
[6] *Institute of Scientific and Industrial Research, Osaka University, Ibaraki, Osaka 567-0047, Japan*
[7] *Department of Physics, Shanghai Jiaotong University, Shanghai 200030, People's Republic of China*
[8] *Neutron Scattering Sciences Division, Oak Ridge National Laboratory, Oak Ridge, Tennessee 37831-6393, USA*

We use inelastic neutron scattering to study the temperature dependence of the spin excitations of a detwinned superconducting $YBa_2Cu_3O_{6.45}$ ($T_c = 48$ K). In contrast to earlier work on $YBa_2Cu_3O_{6.5}$ ($T_c = 58$ K), where the prominent features in the magnetic spectra consist of a sharp collective magnetic excitation termed "resonance" and a large ($\hbar\omega \approx 15$ meV) superconducting spin gap, we find that the spin excitations in $YBa_2Cu_3O_{6.45}$ are gapless and have a much broader resonance. Our detailed mapping of magnetic scattering along the a^*/b^*-axis directions at different energies reveals that spin excitations are unisotropic and consistent with the "hourglass"-like dispersion along the a^*-axis direction near the resonance, but they are isotropic at lower energies. Since a fundamental change in the low-temperature normal state of $YBa_2Cu_3O_{6+y}$ when superconductivity is suppressed takes place at $y \sim 0.5$ with a metal-to-insulator crossover (MIC), where the ground state transforms from a metallic to an insulating-like phase, our results suggest a clear connection between the large change in spin excitations and the MIC. The resonance therefore is a fundamental feature of metallic ground state superconductors and a consequence of high-T_c superconductivity.

I. INTRODUCTION

The parent compounds of the high-transition temperature (high-T_c) copper oxides are Mott insulators characterized by a very strong antiferromagnetic (AF) exchange in the CuO_2 planes and static long-range AF order[1,2,3]. When holes or electrons are doped into the CuO_2 planes, the character of the ground state is fundamentally altered from a Mott insulator with static AF order to a superconductor with persistent short-range AF spin correlations (excitations). If spin excitations are important to the mechanism of superconductivity, they should have universal features for different classes of high-T_c materials and be intimately related to their charge transport properties.

For $YBa_2Cu_3O_{6+y}$ (YBCO) with $y \geq 0.5$, the prominent features in spin fluctuations spectra at the superconducting state include a collective magnetic excitation known as the "resonance" mode, which is sharp in energy and centered at the AF ordering wavevector $Q = (1/2, 1/2)$, and a superconducting spin gap[4,5,6,7,8,9,10,11]. The magnetic excitation spectra show an "hourglass"-like dispersion with the resonance at the saddle point[9,10,11]. The energies of the mode (E_R) and the spin gap (E_{gap}) track T_c's as y is varied, and the opening of the spin gap below T_c is compensated in part by the spectral weight gain of the resonance[4,5,7,8,9,10]. In the case of optimally doped $La_{2-x}Sr_xCuO_4$ (LSCO), inelastic neutron scattering measurements reveal that spin excitations also display an hourglass dispersion with a spin gap and incommensurate resonance below T_c[4,5,12,13]. Although such behavior is remarkably similar to those of optimally doped YBCO and thus suggests a common microscopic origin[4,5], the situation in the underdoped YBCO and LSCO differs quite dramatically. For deeply underdoped $YBa_2Cu_3O_{6.353}$ ($T_c = 18$ K), the spin excitations spectra become gapless and resonance-less; however, they are dominated by commensurate spin excitations and a central diffusive mode associated with a spin-glass phase[14,15,16]. On the other hand, spin excitations in the underdoped $La_{1.875}Ba_{0.125}CuO_4$ are also gapless and resonance-less but display an hourglass dispersion with incommensurate scattering extending to zero energy[5,17,18]. For underdoped superconducting LSCO ($0.055 \leq x \leq 0.125$), spin excitations have clear incommensurability down to the lowest doping of 0.055 and behave similarly as those for $La_{1.875}Ba_{0.125}CuO_4$[19]. Since the resonance appears to be ubiquitous amongst different classes of nearly optimally doped superconducting copper oxides[20,21,22,23], it is important to determine its doping evolution as the mode may be essential to the mechanism of high-T_c superconductivity[24,25,26]. The availability of high quality single crystals of YBCO makes this an ideal system for this study.

To understand the microscopic origin of the differences between YBCO and LSCO, we note that although superconductivity in doped copper oxides first appears when the hole-doping level (x in the case of LSCO) exceeds the critical value of 0.055, a fundamental change in the ground state of these materials in the absence of super-

conductivity actually takes place at much higher doping levels with a metal-to-insulator (MIC) crossover, where the insulating phase under high magnetic fields shows a log $(1/T)$ divergence in resistivity[27]. The MIC happens in the underdoped regime for YBCO around $y = 0.5$[28,29], while it occurs near optimal doping for LSCO ($x \sim 0.16$)[27]. If spin excitations are important in determining the charge transport properties of doped copper oxides, they might respond to the changes in the electronic correlations across the MIC.

To test this idea, we judiciously prepared an underdoped $YBa_2Cu_3O_{6.45}$ [$T_c = 48$ K, Fig. 1(a)] just below the MIC. Although previous work[6,8] have suggested that the spin gap approaches zero for YBCO with y less than about 0.5, it is unclear that such effect is due to oxygen-doping inhomogeneity in the underdoped regime or associated with a MIC because the difficulty in preparing high quality underdoped single crystals with uniform oxygen concentration and sharp T_c. Compared to previous work on $YBa_2Cu_3O_{6.5}$[10], which has a well-defined sharp resonance and a large ($\hbar\omega \approx 15$ meV) superconducting spin gap, our sample has slightly less oxygen content and is in the insulating phase of the MIC. Our inelastic neutron scattering experiments show that the three key features of the excitations spectra: the spin gap, resonance, and hour-glass dispersion in $YBa_2Cu_3O_{6.45}$ are all dramatically different from those in $YBa_2Cu_3O_{6.5}$[10]. Since the MIC for YBCO also occurs near $y = 0.5$, our results thus reveal a clear connection between the quantum spin excitations and the charge transport properties.

II. EXPERIMENT

For our experiments, we used a solute-rich liquid pulling method to grow a large pure YBCO crystal. Compared to the earlier well-studied melt-textured bulk YBCO samples, which contain a significant amount of randomly oriented "green phase" (Y_2BaCuO_5) as an impurity phase[8], these new samples are "green phase" free and have no observable impurity phases. The crystal was cut into four pieces with a total mass of 6 grams and the oxygen content was set to $y = 0.45$ at one atmosphere with 0.5% oxygen partial pressure at 550 °C for 5 days. The samples were mechanically de-twinned at 220 °C and then annealed in sealed tube at 90 °C for more than three weeks to achieve an ordered oxygen state.

Fig. 1(a) plots the magnetic susceptibility of one of the samples showing an onset T_c of 48 K. Based on the empirical T_c vs. oxygen doping plot[30], we estimate that the sample's oxygen content is $y = 0.45$. The inset of Fig. 1(a) shows wavevector scans through (2,0,0) and (0,2,0) Bragg peaks and by fitting these with two Gaussians, we determine the detwinning ratio of 85%. This estimated detwinning ratio can also be checked by intensities of copper oxygen chain (CuO) ordering Bragg peaks. Although the oxygen content is lower than 6.5, the copper oxygen chains can still form the ortho-II super structure[31]. Fig. 1(b) shows ortho-II super lattice peaks at (1/2,0,0) and (0,1/2,0) and the intensity ratio between these two peaks confirms the 85% detwinning ratio.

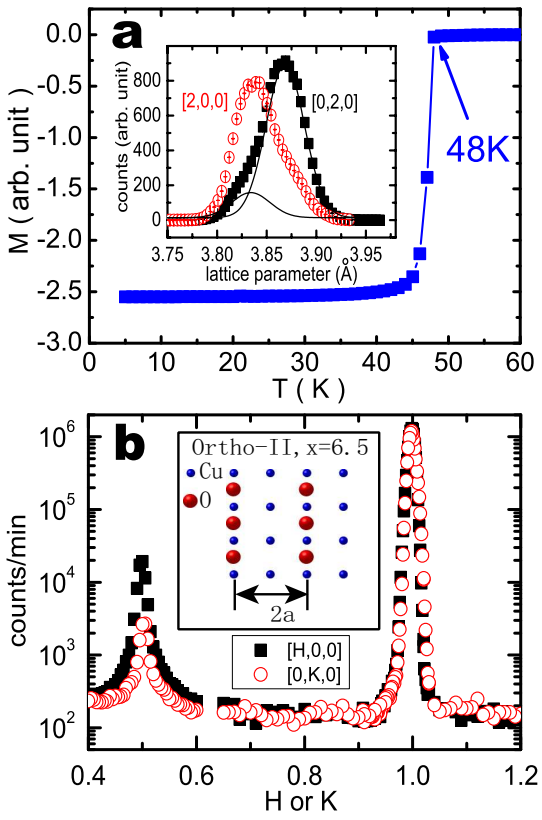

FIG. 1: (a) The temperature dependence of the magnetic susceptibility showing an onset T_c of 48 K with width of 2 K. The inset shows (2,0,0) and (0,2,0) Bragg peaks indicating a detwinning ratio of 85%, as illustrated by the two fitted Gaussian lines for (0,2,0) peak. (b) The ortho-II oxygen ordering (1/2,0,0)/(0,1/2,0) and nuclear (1,0,0)/(0,1,0) peaks. Since the CuO chains form the ortho-II superstructure as shown in the inset, scattering along the a^* direction should result in the (1/2,0,0) peak.

Since our sample has identical ortho-II CuO chain ordering as that of $YBa_2Cu_3O_{6.5}$ but with ∼10 K lower T_c[10], a determination of how the sharp resonance and the large superconducting spin-gap in $YBa_2Cu_3O_{6.5}$ evolves as the system is tuned to $YBa_2Cu_3O_{6.45}$ would reveal the evolution of the intrinsic electronic properties across the MIC without complications from changes in the CuO chain anisotropy. For this purpose, we used inelastic neutron scattering experiments to map out the magnetic scattering function, $S(Q,\omega)$, and then obtain the imaginary part of the dynamic susceptibility,$\chi''(Q,\omega) = S(Q,\omega)(1-e^{-\hbar\omega/k_BT})$, over a range of energies ($0 \leq \hbar\omega \leq 40$ meV) on $YBa_2Cu_3O_{6.45}$ below and above T_c.

The low energy spin excitations were carried out on the cold triple-axis spectrometer SPINS at the NIST Center for Neutron Research (NCNR) with a fixed final neutron energy $E_f = 5$ meV and a cold Be filter before

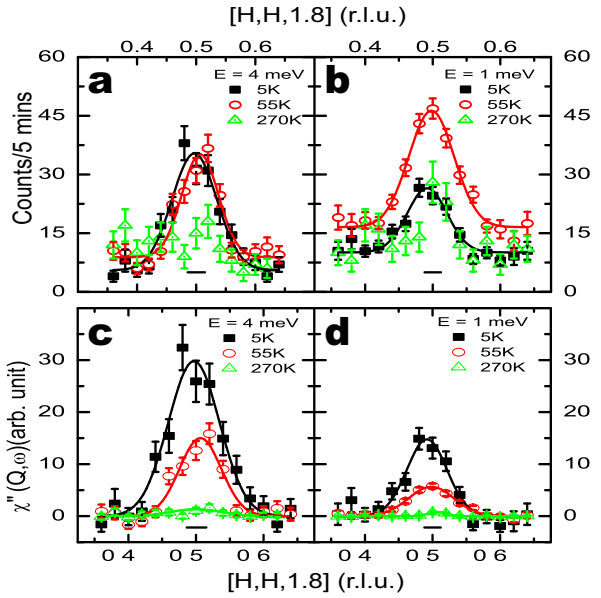

FIG. 2: Q-scans along the $[H, H, 1.8]$ direction at (a) $\hbar\omega = 4$ meV and (b) 1 meV. While the intensity at 4 meV shows no sign of temperature dependence, the intensity at 1 meV clearly increases when the system changes from 5 K to 55 K. The corresponding $\chi''(Q, \omega)$ are shown in (c) and (d), respectively. The horizontal bars are the instrumental resolutions.

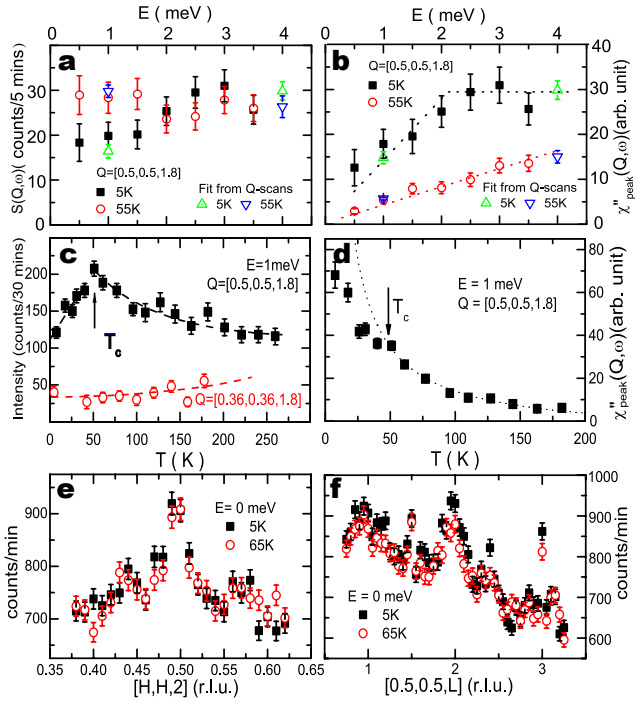

FIG. 3: (a) Energy scans of the difference between $Q = (0.5, 0.5, 1.8)$ and (0.36,0.36,1.8) at 5 K and 55 K. The peak intensities obtained by fitting Q-scans at 1 meV and 4 meV are also plotted. The corresponding dynamic susceptibilities $\chi''(Q, \omega)$ are shown in (b). (c) The temperature dependence of the peak intensity and background at 1 meV. (d) The corresponding $\chi''(Q, \omega)$ of (c). The dotted lines are guided to the eye. (e) Q-scans along the $[H, H, 2]$ direction at $\hbar\omega = 0$ meV and different temperatures. (f) L-scans along the $[0.5, 0.5, L]$ direction at $\hbar\omega = 0$ meV and different temperatures.

the analyzer. The collimations are 60′-open-Sample-80′-open. To study the spin fluctuations at higher energies, we used thermal triple-axis spectrometer C5 at the Canadian Neutron Beam Centre at Chalk River Labs with E_f = 14.7 meV. The collimation for studying resonance and spin dispersion are 30′-48′-Sample-51′-144′ and 30′-28.6′-sample-33.4′-144′, respectively. We denote positions in momentum space using $Q = [H, K, L]$ in reciprocal lattice units (r.l.u.) in which Q [Å^{-1}] = ($H2\pi/a$, $K2\pi/b$, $L2\pi/c$), where $a = 3.834$, $b = 3.869$, and $c = 11.68$ Å.

III. RESULTS

Since superconducting YBCO in the metallic region of MIC (with $y \geq 0.5$) have well-defined low-temperature spin-gaps with $E_{gap} \propto T_c$[8,10] while spin excitations in the low-T_c $YBa_2Cu_3O_{6.353}$ ($T_c = 18$ K) are gapless and resonance-less[15,16], we first probe the possible elastic (quasi-elastic) AF order and low-energy spin excitations in $YBa_2Cu_3O_{6.45}$. The purpose of our measurements is to see if $YBa_2Cu_3O_{6.45}$ has a central diffusive mode similar to those in $YBa_2Cu_3O_{6.353}$.

Fig. 2(a) and 2(b) show the $S(Q, \omega)$ in Q-scans along the $[H, H, 1.8]$ direction at $\hbar\omega = 4$ meV and 1 meV respectively, where $L = 1.8$ r.l.u. is the maximum intensity position for the acoustic spin excitations of the bilayer YBCO[6,7,8,9,10]. It is clear that the excitations at 4 meV show no temperature dependence when the system changes from the low temperature superconducting state ($T = 5$ K) to the high temperature normal state ($T = T_c + 7$ K). However, the $S(Q, \omega)$ peak intensity for $\hbar\omega = 1$ meV is larger at $T = 55$ K than that at 5 K. Fig. 2(c) and 2(d) plot the corresponding $\chi''(Q, \omega)$ obtained from data in Figs. 2(a) and 2(b) respectively. The dynamic susceptibility at both energies decrease with the increase of temperatures, which indicates a gapless low-temperature ground state.

To further study the low energy spin fluctuations, we measured the energy dependence of the scattering at the peak $Q = (0.5, 0.5, 1.8)$ and background $Q = (0.36, 0.36, 1.8)$ positions for the acoustic mode[6,7,8,9,10]. The scattering function $S(Q, \omega)$ at different temperatures can then be estimated by subtracting the background scattering from the peak position as shown in Fig. 3(a). Although the statistics of the subtracted data can still be improved, it is clear that the $S(Q, \omega)$ below 2 meV decreases as the system enters into the superconducting state from the normal state. Constant-energy scans at $\hbar\omega = 1$ and 4 meV below and above T_c shown in Figs. 2(a) and 2(b) confirm the result of Fig. 3(a). Fig. 3(b) shows the $\chi''(Q, \omega)$ at 5 and 55 K obtained using $S(Q, \omega)$ and constant-energy scans in

Fig. 3(a). While the $\chi''(Q,\omega)$ at 55 K increases linearly with $\hbar\omega$, consistent with the energy dependence of the normal state dynamics susceptibility in other metallic ground state YBCO[7,8,10], it is clear that the $\chi''(Q,\omega)$ is gapless in the low-temperature superconducting state and shows a characteristic energy scale around 2.0 meV. This energy scale is similar to those found in the deeply underdoped $YBa_2Cu_3O_{6.353}$[15,16] and electron-doped superconducting $Pr_{0.88}LaCe_{0.12}CuO_4$ with $T_c = 21$ K[32]. However, in contrast to $YBa_2Cu_3O_{6.353}$[15,16], extensive searches in our samples have failed to find any static (or quasielastic) AF order or the central mode. Fig. 3(e) gives Q-scans along the $[H,H,2]$ direction, which is the position expected for the central diffusive mode[15]. The lack of temperature dependence between 5 K and 65 K indicates that the scattering is nonmagnetic. In addition, the L-scans along the $[0.5,0.5,L]$ direction shown in Fig. 3(f) do not follow the lattice periodicity as those in $YBa_2Cu_3O_{6.353}$[15]. From previous work on underdoped YBCO with a central mode[15,16,33], we know that the intensity of the central mode decreases rather rapidly with increasing hole doping and should certainly be present below 65 K in our $YBa_2Cu_3O_{6.45}$. A comparison with a recent μSR results[14] suggests that our sample might be close to the magnetic quantum critical point resulting from the spin-glass phase. We also note that the low energy scale around 2.0 meV in our sample is in the superconducting state, different from those in the lower-doping YBCO[15,16,33].

If the intensity reduction below 2 meV in Fig. 3(a) is indeed related to the bulk superconductivity, one should expect that the temperature dependent scattering should respond to superconductivity. Fig. 3(c) shows the temperature dependence measurements at the peak $Q = (0.5,0.5,1.8)$ and background $Q = (0.36,0.36,1.8)$ positions for $\hbar\omega = 1$ meV. The scattering at the peak position initially increases, but then drops substantially below T_c showing a clear kink at T_c. On the other hand, the background scattering shows no observable anomaly across T_c as shown in Fig. 3(c). Fig. 3(d) plots the temperature dependence of the $\chi''(Q,\omega)$ at 1 meV, obtained by subtracting the background from the signal scattering and correcting for the Bose population factor. The $\chi''(Q,\omega)$ increases with the decreasing temperature, but shows a clear kink at T_c. The fact that the $\hbar\omega = 1$ meV spin excitations respond to the occurrence of superconductivity effectively rules out the possibility that the low-energy spin excitations arise from the sample oxygen inhomogeneity. In the latter case, one would not expect the low energy spin fluctuations responding to the bulk superconductivity.

To search for the magnetic resonance in $YBa_2Cu_3O_{6.45}$, we note that the intensity of the resonance increases below T_c like an order parameter and its energy tracks T_c as the oxygen composition is varied via $E_R = 5.8\ k_BT_c$[7,8,10,22]. Since $YBa_2Cu_3O_{6.45}$ has a $T_c = 48$ K, we expect the mode to occur at energies around 20 meV. Fig. 4(a) shows energy

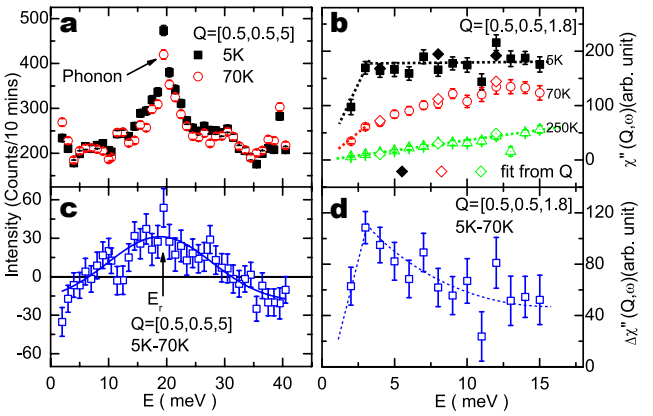

FIG. 4: (a) Energy-scans at $Q = (0.5,0.5,5)$ taken below (5 K) and above (70 K) T_c. The difference in (c) shows a clear peak centered around 20 meV with a FWHM of 15 meV. (b) Temperature dependence of the dynamic susceptibility at the equivalent position $Q = (0.5,0.5,1.8)$ showing clear magnetic intensity gain on cooling. The low-energy dashed lines are from fits in Fig. 3(b). (d) The temperature difference in dynamic susceptibility.

scans at wavevector $Q = (0.5,0.5,5)$ below (5 K) and above (70 K) T_c. Consistent with earlier results on higher-doping YBCO[7,8,10], the raw data are dominated by phonon scattering at 20 meV and 30 meV at both temperatures. However, when one takes the temperature difference spectra below and above T_c, a broad peak with a full-width-half-maximum (FWHM) of ~ 15 meV emerges at $\hbar\omega \approx 19$ meV [Fig. 4(c)]. Since intensity of phonons should decrease with decreasing temperature and the Bose population factor does not much affect the magnetic scattering above 10 meV for temperatures from 5 to 70 K, the net intensity gain in Fig. 4(a) must be the result of enhanced dynamic susceptibility below T_c. Although such intensity gain below T_c is a hallmark of the resonance, the observed broad energy peak is quite different from the instrumental resolution-limited resonance for YBCO at higher doping levels[7,8,10].

To see if the intensity gain below T_c is consistent with the bilayer Cu^{2+} acoustic magnetic excitations from YBCO, we carried out energy scans at the equivalent acoustic wavevector $Q = (0.5,0.5,1.8)$. The energy dependence of the susceptibilities $\chi''(Q,\omega)$ at different temperatures are summarized in Fig. 4(b), where the average values of intensities at $Q = (0.3,0.3,1.8)$ and (0.7,0.7,1.8) have been used as background. Consistent with the cold neutron data in Fig. 3, $\chi''(Q,\omega)$ is proportional to $\hbar\omega$ above T_c, and increases with decreasing temperature. The difference spectrum $\Delta\chi''(Q,\omega)$ between 5 K and 70 K in Fig. 4(d) shows a clear kink around 2 meV in susceptibility consistent with the cold neutron data in Fig. 3(b). Note that the $\chi''(Q,\omega)$ is the peak susceptibility at $Q = (0.5,0.5,1.8)$. To obtain the local susceptibility $\chi''(\omega)$ at different energies, one must carry out wavevector integration considering the detailed dispersion of spin

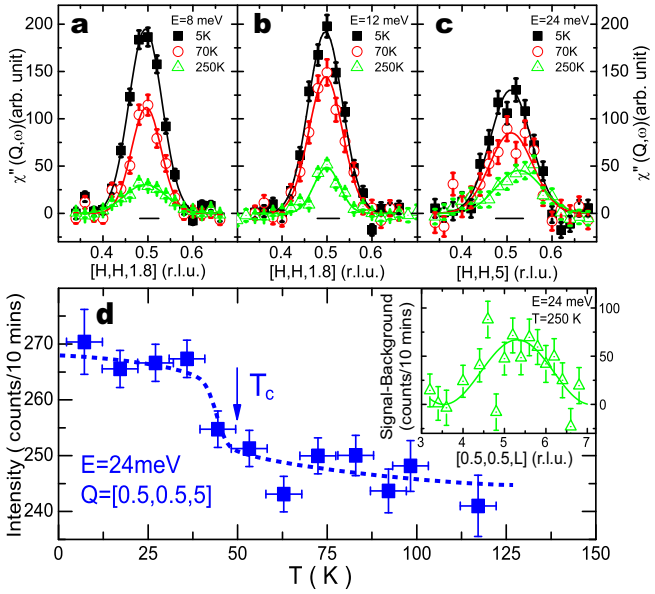

FIG. 5: (a)-(c) Wavevector dependence of dynamic susceptibility along the $[H, H]$ direction at different energies and temperatures. There are clear magnetic scattering consistent with acoustic magnetic scattering structure factor even at 250 K, as shown in the inset of (d). (d) The temperature dependence of the scattering at 24 meV and (0.5,0.5,5) shows an order-parameter-like increase below T_c, a hallmark of the resonance.

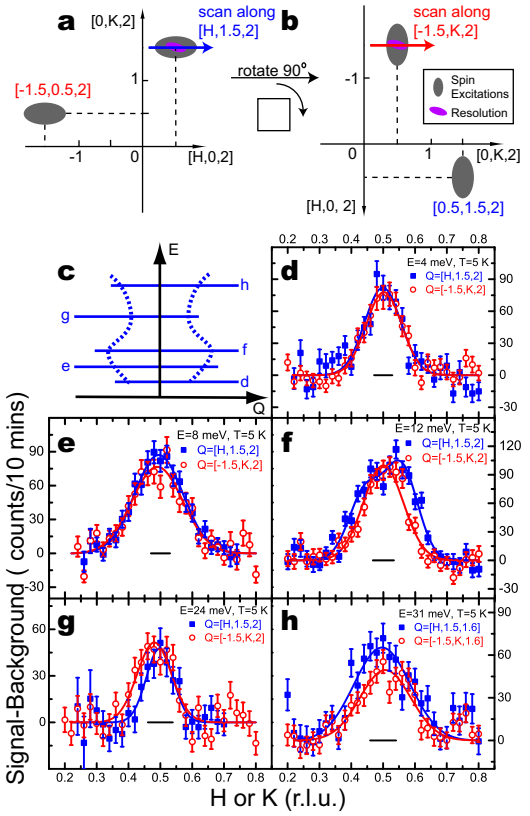

FIG. 6: (a,b) Experimental setup for studying magnetic anisotropy in our $YBa_2Cu_3O_{6.45}$. The measurements were carried out in the $[H, K, 4K/3]$ and $[H, K, 4H/3]$ zones by rotating the sample 90 degrees along the c^*-axis. The advantage of such a setup is that the instrumental resolutions are identical in the a^* and b^* scan directions. (c) Schematic Q-scans at different energies. (d)-(h), Q-scans along the $[H, 1.5, 2]$ and $[-1.5, K, 2]$ directions at different energies in the low-temperature superconducting state. While the scattering profiles are commensurate and isotropic at 4 and 8 meV, clear anisotropic scattering appears at 12 meV. The data show clear flattish top. The Q-profiles become narrow and isotropic again near the resonance energy. The instrumental resolutions are shown as the horizontal bars.

excitations. Although $\Delta\chi''(\omega)$ still shows a broad peak around 2 meV after considering the Q-width below T_c, the temperature dependence of the magnetic scattering at 2 meV shows no direct correlation with T_c and therefore differs from the neutron spin resonance at $\hbar\omega \approx 19$ meV.

Fig. 5(a)-(c) show wavevector dependence of $\chi''(Q, \omega)$ at $\hbar\omega = 8$, 12, and 24 meV below and above T_c. Inspection of Figure reveals that the superconductivity-induced susceptibility gain increases from 12 to 24 meV, and there is substantial magnetic scattering even at 250 K. In order to confirm that the observed scattering at 250 K is from acoustic magnetic excitations in YBCO, we carried out Q-scans along the c-axis direction. The L-modulation of the $\hbar\omega = 24$ meV excitation at 250 K [inset in Fig. 5(d)] follows the expected acoustic bilayer structure factor, which is proportional to $sin^2(\pi dL)$ (d is the distance between CuO_2 planes within a bilayer unit)[7,8,10]. Finally, the temperature dependence of the scattering at $Q = (0.5, 0.5, 5)$ and $\hbar\omega = 24$ meV shows an order parameter-like increase below T_c similar to the temperature dependence of the resonance in the higher-doping YBCO. These results thus demonstrate that the broad peak centered at $\hbar\omega = 19$ meV is indeed the magnetic resonance similar to other superconducting cuprates.

Having shown the presence of the resonance in our $YBa_2Cu_3O_{6.45}$, it is important to determine its dispersion as the outcome will allow a direct comparison of the magnetic spectra between underdoped YBCO and LSCO. Previous neutron scattering work on YBCO with $y = 0.5$, and 0.6 have shown that the dispersion of the resonance has an hourglass shape[9,10], with incommensurate scattering below the resonance being anisotropic, having a magnetic anisotropy with a larger incommensurability along the a^*-axis direction than the b^*-axis direction[34,35,36]. Since the low-energy spin fluctuations in our $YBa_2Cu_3O_{6.45}$ are commensurate, it will be interesting to determine the dispersion of spin excitations along H and K directions near the resonance. To accomplish this, we co-aligned the samples in either the $[H, K, 4/3K]$ or $[H, K, 4/3H]$ zone by simply rotating them 90 degrees along the c^*-axis in the $[H, K, 0]$ zone before tilting around the $a^*(b^*)$-axis. The unique advantage

of such experimental geometries is that one can carry out scans along the $[H, 1.5, 2]$ or $[-1.5, K, 2]$ directions with identical instrumental resolution, thus allowing a direct comparison of the possible magnetic anisotropy in this material [Fig. 6(a) and 6(b)].

Fig. 6(d)-6(h) summarize the constant-energy scans along H and K directions for energy transfers of $\hbar\omega = 4$, 8, 12, 24, and 31 meV in the low temperature superconducting state. At $\hbar\omega = 4$ meV, Q-scans along the H and K directions show identical behavior and suggest that spin fluctuations are isotropic at this energy [Fig. 6(d)]. On increasing the energy to $\hbar\omega = 8$ meV, the excitations become broader in Q but are still the same along H and K directions [Fig. 6(e)]. Upon increasing the energy further to $\hbar\omega = 12$ meV, the Q-scan along the H direction shows a clear flattish top indicative of incommensurate spin excitations while the identical scan along the K direction is commensurate and has a smaller width than the Q-scan along the a^* direction. We fit the data with two Gaussian peaks with the incommensurability of $\delta = 0.057 \pm 0.003$ r.l.u. being consistent with the universal δ vs T_c plot[8]. At energies near and above the resonance (at $\hbar\omega = 24$, and 31 meV, respectively), the scattering profiles become narrow again and the in-plane magnetic anisotropy essentially disappears [Figs. 6(g) and 6(h)]. Our results above 12 meV are consistent with an hourglass dispersion and display a weak anisotropy below the resonance, similar to the previous results at higher doping[34,35,36], but the low energy excitations become isotropic.

To obtain the integrated $\chi''(\omega)$, one must carry out two-dimensional wavevector integration of $\chi''(Q, \omega)$ within the $[H, K]$ plane. Since we did not carried out detailed Q-scans over a wide energy range and it is difficult to separate magnetic scattering from phonons around 20 meV, we have not attempted to construct a $\chi''(\omega)$ versus $\hbar\omega$ plot similar to those for YBCO[10,11] and LSCO[12,13].

IV. DISCUSSIONS AND CONCLUSIONS

Figure 7 summarizes our present results together with schematics of dispersions from previous work on YBCO and LSCO. Figures 7(a) and 7(b) show the low-temperature spin-gap and resonance energies as a function of T_c for YBCO[7,8,10,15]. Figures 7(c-e) illustrate the observed spin excitation dispersions for LSCO and YBCO with different ground states. Figure 7(f) plots the dispersions of the spin excitations along the a^*-direction. The disappearing spin gap energy in the sample did not reveal more incommensurate scattering as expected in Fig. 7(e) from a naïve stripe picture but instead showed that the low-energy spin excitations are commensurate much different from the dispersion of the lower-doping LSCO.

The surprising discovery of disappearing spin gap and isotropic spin fluctuations below the hourglass dispersion suggests that the doping evolution of spin excitations

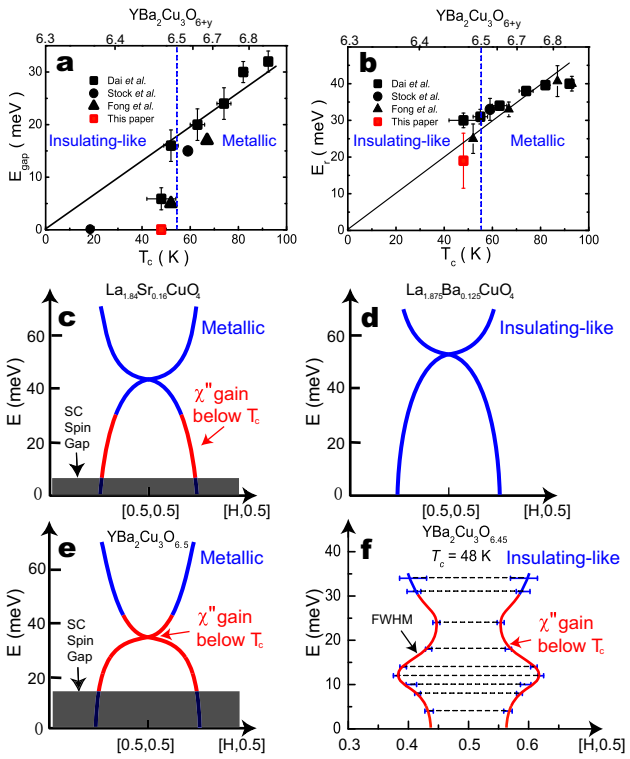

FIG. 7: (a) Spin gap energies as a function of T_c for YBCO. There is a sudden reduction below $y = 0.5$ and the MIC. (b) The resonance energies and their widths as a function of T_c for YBCO. The energy width of the resonance increases dramatically below $y = 0.5$ and the MIC. (c) The schematic dispersion for optimally doped $La_{1.84}Sr_{0.16}CuO_4$. On cooling below T_c, a clean spin gap (about 6 meV) opens and the spectral weight shifts from below to above the gap as shown in red region[12,13]. (d) The schematic dispersion for static stripe ordered $La_{1.875}Ba_{0.125}CuO_4$, where incommensurate spin fluctuations extend to zero energy and there is no spectral weight enhancement below T_c[17,18]. (e) Dispersion of YBCO for $y \geq 0.5$. The low-energy incommensurate scattering were obscured by the presence of the low-temperature spin gap. The lines within the gap indicate the expected dispersion from a naïve stripe model for $y < 0.5$ samples[5]. (f) Observed dispersion for $YBa_2Cu_3O_{6.45}$ along the a^* direction. The part above 12meV is consistent with an hourglass like dispersion, which breaks down at low-energies.

in LSCO and YBCO families of cuprates is quite different. The dramatic increase in the magnitude of the spin gap and the width narrowing of the resonance on moving from $y = 0.45$ to 0.5 in YBCO's with ortho-II CuO chain ordering [Fig. 7(a) and 7(b)] suggest that these changes in spin dynamical properties are related with the MIC and its associated quantum phase transition. Since the oxygen concentration in YBCO is difficult to determine precisely, the relationship between T_c's and the oxygen contents differ slightly by different groups[28,29,30]. The oxygen contents in Figs. 7(a) and 7(b) are calculated based on the empirical results reported by Liang *et al.*[30]. In the original work of Dai *et al.*[8], spin exci-

tations of an underdoped twinned melt-textured sample of $YBa_2Cu_3O_{6.45}$ were found to have a spin gap of 6 meV and a sharp resonance at 30 meV. Although the T_c of this sample was reported to also be $T_c = 48$ K, the transition width is about 12 K and T_c is defined to be the middle point in the DC susceptibility measurement[8]. This means that the oxygen concentration in the earlier melt-textured $YBa_2Cu_3O_{6.45}$ is much less homogeneous. As a consequence, the observed resonance and spin-gap in the melt-textured $YBa_2Cu_3O_{6.45}$ may arise from portion of the sample with higher T_c. In any case, the spin excitations at 10 meV from the earlier experiments also show a tendency of commensurate scattering below the incommensurate peaks at 16 meV[8].

Since recent transport measurements have demonstrated the presence of Fermi pockets in the high-field vortex state of $YBa_2Cu_3O_{6.5}$[37], we speculate that the sharp resonance and clean spin gap are fundamental properties of metallic ground state copper oxides. Indeed, such speculation is also consistent with the data in LSCO, where one finds a clean spin gap and incommensurate "resonance" – or more precisely, susceptibility gain below T_c – near optimal Sr-doping in the metallic phase[12,13,38] but fails to detect any signature of a clean spin gap or resonance in underdoped materials in the insulating-like phase[17,18,39].

Our results present new challenges to the two current competing theories explaining the microscopic origin of the spin excitations. In one school of thought, doped holes in the CuO_2 are phase separated from the AF insulating background and self-organize into metallic "stripes", which necessitates unconventional superconductivity[40,41]. Neutron scattering experiments on $La_{1.875}Ba_{0.125}CuO_4$, where superconductivity is suppressed by the static stripes, have shown that spin excitations form an hourglass dispersion (Fig. 7d) with low-energy incommensurate peaks (measuring spacing between stripes) merge into a saddle point determined by the interactions between stripes[17,18]. In this picture, incommensurate spin excitations in the superconducting LSCO and YBCO arise from dynamic stripes[5] and the MIC itself is not expected to much affect the stripe correlations[40,41]. Our observation of the narrowing commensurate spin excitations below the hourglass resonance in $YBa_2Cu_3O_{6.45}$ [Fig. 7(f)] is inconsistent with the naïve picture of stripe correlations. If stripe correlations were to explain the observed spectra, something more exotic, for example the electronic nematic phase[42], might be required to become important below the MIC for YBCO[28,29]. In fact, the transport measurements in YBCO by Ando *et al.*[28] had found an increase in the resistivity anisotropy between the a and b directions with the decreasing doping attributed to the "striped" or electronic nematic phase. Ignoring the quoted oxygen concentrations as these may differ from group to group[29,30], we find that the resistivity anisotropy becomes much smaller for samples with $T_c \approx 50$ K, consistent with our observation of isotropic spin excitations at low energies [Fig. 7(f)]. If this scenario is indeed correct, one would expect that the low-energy spin excitations to become anisotropic for YBCO samples with lower T_c and oxygen content.

Alternatively, the resonance and incommensurate spin excitations around it can be explained by quasiparticle scattering across a nested Fermi surface as in conventional metals and superconductors[43,44]. Based on this approach, a rapid reduction in the magnitude of the spin gap and the near-disappearance of the resonance in the $YBa_2Cu_3O_{6.45}$ suggests a sudden change in the Fermi surface topology across the MIC in YBCO[45]. Although recent experiments[37] have demonstrated the presence of Fermi pockets in the metallic side of the MIC in the vortex state, it is still unclear what happens to the Fermi surface or if there are any Fermi surfaces at all in the insulating-like regime below the MIC. In any case, a microscopic understanding of the spin excitations[4,5] and in-plane anisotropy[40,41] will require new theoretical work that takes into account the differences on emergence of the hourglass dispersions between LSCO and YBCO with increasing doping. Our data provided the missing link in this comparison, and reveal that the resonance and spin gap are fundamental properties of metallic ground state hole-doped superconductors.

Very recently, Rullier-Albenque *et al.*[46] suggested a new microscopic interpretation on the MIC, where the differences in out-of-plane lattice disorder between YBCO and LSCO are used to explain why the MIC takes place at different hole-doping levels for these two materials. Since disorder is known to induce in-gap states and low-energy spin excitations[47], one might speculate that the diorder in our $YBa_2Cu_3O_{6.45}$ is considerably larger than those in the $YBa_2Cu_3O_{6.5}$[10]. In this picture, the large reduction in the spin-gap energy and the broadening of the resonance below the MIC is induced by the sudden increase in the lattice disorder in $YBa_2Cu_3O_{6.45}$. Although we cannot exclude the possible existence of nano-scale defects or intrinsic disorder, the presence of well-established ortho-II order in our sample suggests that such defects and disorder do not dominate the Cu-O chain order. If disorder indeed plays an important role in the spin dynamics of YBCO with oxygen content near 6.5, one would expect to observe large changes in spin excitations as the oxygen chain order in the ortho-II $YBa_2Cu_3O_{6.45}$ is quenched into the ortho-I phase. Work is currently underway to study the oxygen disorder effects on spin dynamics in $YBa_2Cu_3O_{6.45}$.

Acknowledgments

We thank W. J. L. Buyers and Elbio Dagotto for helpful discussions. This work is supported by the U.S. DOE BES under grant No. DE-FG02-05ER46202. ORNL is supported by the U.S. DOE under contract No. DE-AC05-00OR22725 through UT/Battelle LLC. Works at SJTU and CRIEPI are supported by the MOST of China

(973 project No. 2006CB601003) and the Grant-in-Aid for Science provided by the Japan Society for the Promotion of Science, respectively.

* Electronic address: slli@utk.edu
† Electronic address: daip@ornl.gov

[1] J. Orenstein and A. J. Millis, Science **288**, 5465 (2000).
[2] A. Abanov, A. V. Chubukov, and J. Schmalian, J. Electron Spectrosc. Relat. Phenom. **117-118**, 129 (2001).
[3] D. J. Scalapino, Phys. Rep. **250**, 330 (1995).
[4] R. J. Birgeneau, C. Stock, J. M. Tranquada, and K. Yamada, J. Phys. Soc. Jpn. **75**, 111003 (2006).
[5] J. M. Tranquada, in *Handbook of High-Temperature Superconductivity*, edited by J. R. Schrieffer and J. S. Brooks (Springer, New York, 2007), p. 257.
[6] L. P. Regnault, P. Bourges, P. Burlet, J. Y. Henry, J. Rossat-Mignod, Y. Sidis, and C. Vettier, Physica B **213-214**, 48 (1995).
[7] H. F. Fong, P. Bourges, Y. Sidis, L. P. Regnault, J. Rossy, A. Ivanov, D. L. Milius, I. A. Aksay, and B. Keimer, Phys. Rev. B **61**, 14773 (2000).
[8] Pengcheng Dai, H. A. Mook, R. D. Hunt, and F. Doğan, Phys. Rev. B **63**, 054525 (2001).
[9] S. M. Hayden, H. A. Mook, P. Dai, T. G. Perring, and F. Doğan, Nature **429**, 531 (2004).
[10] C. Stock, W. J. L. Buyers, R. Liang, D. Peets, Z. Tun, D. Bonn, W. N. Hardy, and R. J. Birgeneau, Phys. Rev. B **69**, 014502 (2004).
[11] H. Woo, P. Dai, S. M. Hayden, H. A. Mook, T. Dahm, D. J. Scalapino, T. G. Perring, and F. Doğan, Nat. Phys. **2**, 600 (2006).
[12] N. B. Christensen, D. F. McMorrow, H. M. Rϕnnow, B. Lake, S. M. Hayden, G. Aeppli, T. G. Perring, M. Mangkorntong, M. Nohara, and H. Takagi, Phys. Rev. Lett. **93**, 147002 (2004).
[13] B. Vignolle, S. M. Hayden, D. F. McMorrow, H. M. Rϕnnow, B. Lake, C. D. Frost, and T. G. Perring, Nat. Phys. **3**, 163 (2007).
[14] J. E. Sonier, F. D. Callaghan, Y. Ando, R. F. Kiefl, J. H. Brewer, C. V. Kaiser, V. Pacradouni, S. A. Sabok-Sayr, X. F. Sun, S. Komiya, *et al.*, Phys. Rev. B **76**, 064522 (2007).
[15] C. Stock, W. J. L. Buyers, Z. Yamani, C. L. Broholm, J.-H. Chung, Z. Tun, R. Liang, D. Bonn, W. N. Hardy, and R. J. Birgeneau, Phys. Rev. B **73**, 100504(R) (2006).
[16] C. Stock, R. A. Cowley, W. J. L. Buyers, R. Coldea, C. L. Broholm, C. D. Frost, R. J. Birgeneau, R. Liang, D. Bonn, and W. N. Hardy, Phys. Rev. B **75**, 172510 (2007).
[17] J. M. Tranquada, H. Woo, T. G. Perring, H. Goka, G. D. Gu, G. Xu, M. Fujita, and K. Yamada, Nature **429**, 534 (2004).
[18] G. Xu, J. M. Tranquada, T. G. Perring, G. D. Gu, M. Fujita, and K. Yamada, Phys. Rev. B **76**, 014508 (2007).
[19] K. Yamada, C. H. Lee, K. Kurahashi, J. Wada, S. Wakimoto, S. Ueki, H. Kimura, Y. Endoh, S. Hosoya, G. Shirane *et al.*, Phys. Rev. B **57**, 6165 (1998).
[20] H. F. Fong, P. Bourges, Y. Sidis, L. P. Regnault, A. Ivanov, G. D. Gu, N. Koshizuka, and B. Keimer, Nature (London) **398**, 588 (1999).
[21] H. He, P. Bourges, Y. Sidis, C. Ulrich, L. P. Regnault, S. Pailhes, N. S. Berzigiarova, N. N. Kolesnikov, and B. Keimer, Science **295**, 1045 (2002).
[22] S. D. Wilson, Pengcheng Dai, Shiliang Li, S. X. Chi, H. J. Kang, and J. W. Lynn, Nature (London) **442**, 59 (2006).
[23] Jun Zhao, Pengcheng Dai, Shiliang Li, P. G. Freeman, Y. Onose, and Y. Tokura, Phys. Rev. Lett. **99**, 017001 (2007).
[24] E. Demler and S.-C. Zhang, Nature (London) **396**, 733 (1998).
[25] Pengcheng Dai, H. A. Mook, S. M. Hayden, G. Aeppli, T. G. Perring, R. D. Hunt, F. Doğan, Science **284**, 1344 (1999).
[26] S. D. Wilson, Shiliang Li, Jun Zhao, G. Mu. H.-H. Wen, J. W. Lynn, P. G. Freeman, L. P. Regnault, K. Habicht, and Pengcheng Dai, PNAS **104**, 15259 (2007).
[27] G. S. Boebinger, Y. Ando, A. Passner, T. Kimura, M. Okuya, J. Shimoyama, K. Kishio, K. Tamasaku, N. Ichikawa, and S. Uchida, Phys. Rev. Lett. **77**, 5417 (1996).
[28] Y. Ando, K. Segawa, S. Komiya, and A. N. Lavrov, Phys. Rev. Lett. **88**, 137005 (2002).
[29] X. F. Sun, K. Segawa, and Y. Ando, Phys. Rev. Lett. **93** 107001 (2004).
[30] R. Liang, D. A. Bonn, and W. N. Hardy, Phys. Rev. B **73**, 180505(R) (2006).
[31] N. H. Andersen, M. von Zimmermann, T. Frello, M. Käll, D. Mϕnster, P. A. Lindgård, J. Madsen, T. Niemöller, H. F. Poulsen, O. Schimidt, *et al.*, Physica C **317-318**, 259 (1999).
[32] S. D. Wilson, S. Li, H. Woo, P. Dai, H. A. Mook, C. D. Frost, S. Komiya, and Y. Ando, Phys. Rev. Lett. **96**, 157001 (2006).
[33] Z. Yamani, W. J. L. Buyers, F. Wang, Y.-J. Kim, R. Liang, D. Bonn and W.N. Hardy, Physica C **460-462**, 430 (2007).
[34] H. A. Mook, P. Dai, F. Doğan, and R. D. Hunt, Nature **404**, 729 (2000).
[35] V. Hinkov, S. Pailhès, P. Bourges, Y. Sidis, A. Ivanov, A. Kulakov, C. T. Lin, D. P. Chen, C. Bernhard, and B. Keimer, Nature **430**, 650 (2004).
[36] V. Hinkov, P. Bourges, S. Pailhès, Y. Sidis, A. Ivanov, C. D. Frost, T. G. Perring, C. T. Lin, D. P. Chen and B. Keimer, Nature Physics **3**, 780 (2007).
[37] N. Doiron-Leyraud, C. Proust, D. LeBoeuf, J. Levallois, J.-B. Bonnemaison, R. Liang, D. A. Bonn, W. N. Hardy, and L. Taillefer, Nature **447**, 565 (2007).
[38] J. M. Tranquada, C. H. Lee, K. Yamada, Y. S. Lee, L. P. Regnaut, and H. M. Rϕnnow, Phys. Rev. B **69**, 174507 (2004).
[39] J. Chang, A. P. Schnyder, R. Gilardi, H. M. Rϕnnow, S. Pailhes, N. B. Christensen, C. Niedermayer, D. F. McMorrow, A. Hiess, A. Stunault, *et al.*, Phys. Rev. Lett. **98**, 077004 (2007).
[40] S. A. Kivelson, I. P. Bindloss, E. Fradkin, V. Oganesyan, J. M. Tranquada, A. Kapitulnik, and C. Howald, Rev. Mod. Phys. **75**, 1201 (2003).
[41] J. Zaanen, O. Y. Osman, H. V. Kruis, Z. Nussinov, and J. Torzydlo, Philos. Mag. B **81**, 1485 (2001).
[42] S. A. Kivelson, E. Fradkin, and V. J. Emery, Nature **393**, 550 (1998).
[43] M. Eschrig, Adv. Phys. **55**, 47 (2006).
[44] M. R. Norman, Phys. Rev. B **75**, 184514 (2007).

[45] F. Onufrieva, S. Petit, and Y. Sidis, Phys. Rev. B **54**, 12464 (1996).
[46] F. Rullier-Albenque, H. Alloul, F. Balakirev and C. Proust, arXiv:0710.3737v1.
[47] H. Alloul, J. Bobroff, M. Gabay and P. J. Hirschfeld, arXiv:0710.3737v1, and references therein.